



Structural, electronic, magnetic, and thermoelectric properties of half Heusler alloys $ZrCo_{1-x}Fe_xSb$ ($X = 0, 0.25, 0.5, 0.75, 1$): A DFT study

R. Meenakshi^b, R. Aram Senthil Srinivasan^c, A. Amudhavalli^d, K. Iyakutti^e, Y. Kawazoe^{e,f}, R. Rajeswara Palanichamy^{a,*}

^a Department of Physics, N.M.S.S. Vellaichamy Nadar College, Madurai, Tamilnadu, 625019, India

^b Department of Physics, Government College of Engineering, Tirunelveli, Tamilnadu, 627007, India

^c Department of Basic Engineering, Government Polytechnic College, Thoothukudi, Tamilnadu, 628008, India

^d Department of Physics, Indian Institute of Technology, Madras, Tamilnadu, 600 036, India

^e Department of Physics and Nanotechnology, SRM Institute of Science and Technology, Kattankulathur, Chennai, Tamilnadu, 603203, India

^f New Industry Creation Hatchery Center (NICHe), Tohoku University, Sendai, 980-8579, Japan

ARTICLE INFO

Keywords:

First-principles calculations
Half Heusler alloys
Half-metallic
Electronic structure
Magnetic
Thermoelectric properties

ABSTRACT

The structural, electronic, magnetic, and thermoelectric properties of half-Heusler alloys $ZrCo_{1-x}Fe_xSb$ ($X = 0, 0.25, 0.5, 0.75, 1$) are investigated using the density functional theory. It is evident that $ZrCoSb$ is a non-magnetic semiconductor. This study investigates the influence of substituting Fe for Co on the electronic structure and magnetic characteristics of $ZrCoSb$. The alloys transform into half-metallic ferromagnets as Fe substitutes Co. The indirect band gap of the $ZrCo_{1-x}Fe_xSb$ alloys decreases with increasing Fe content. The phonon dispersion curve is studied to determine the structural stability. The calculated values for the elastic constant for each composition satisfy the criteria for mechanical stability. To analyse its thermoelectric properties, the semi-classical Boltzmann transport theory is used to determine the Seebeck coefficients, electrical and thermal conductivities, and power factor as a function of temperature.

1. Introduction

Fritz Heusler discovered a novel form of intermetallic compounds known as Heusler alloys in 1930 [1]. The magnetic properties exhibited by the Heusler alloy make it very suitable for use in various applications such as spintronics [2–7], spin filters [8], magnetic tunnel junctions [9, 10], and magnetic storage systems [11]. Furthermore, the significance of these materials has been amplified in recent years as a result of their interesting use in superconductors [12] and thermoelectric materials [13–16] employed in various fields, including waste heat recovery and power generation in space. Heusler alloys are X_2YZ alloy composed of four fcc sublattices in the crystal structure L2₁. When one X sub lattice is replaced by vacancies, an XYZ alloy with a C1_b structure is formed, which is known as a half-Heusler alloy. Half-Heusler alloys MCoSb (M = Ti, Zr, Hf) have cubic MgAgAs type structure. These alloys, with the space group F4-3m (No. 216), are semiconductors with a narrow band gap [17, 18]. Several theoretical and experimental studies have been done on the thermoelectric characteristics of the $ZrCoSb$ alloy [19–22]. It has been reported that $ZrCoSb$ shows non-magnetic semiconducting

properties. The structural, elastic, and half-metallic characteristics of FeZrX ($X = P, As, Sb$ and Bi) half-Heusler compounds have been examined by Özdemir EG and Merdan Z [23] using the WIEN2k code. Several half-metallic ferromagnetic and thermoelectric materials have been produced by optimal substitution or doping with Zr-based Heusler alloys [24–32]. Despite studies on a variety of Zr-based Heusler alloys, new thermoelectric and spintronic materials are still necessary.

In this paper, we investigate the structural, electronic, magnetic, and thermoelectric properties of the $ZrCo_{1-x}Fe_xSb$ ($X = 0, 0.25, 0.5, 0.75, 1$) half-Heusler alloys, since there is no theoretical or experimental study on $ZrCo_{1-x}Fe_xSb$ ($X = 0.25, 0.5, 0.75$) alloys. In this paper, the effects of the substitution of Fe atoms for Co atoms on the structure, magnetic properties, electronic properties, HM characters, and thermoelectric properties of $ZrCo_{1-x}Fe_xSb$ ($X = 0, 0.25, 0.5, 0.75, 1$) alloy, as well as its suitability for thermoelectric and spintronics applications, are analysed.

2. Theoretical framework

In this study, we employed the Wien2k code [33] within the

* Corresponding author. Department of Physics, N.M.S.S.V.N College, Madurai, Tamilnadu, 625019, India.

E-mail address: rrpalanichamy@gmail.com (R. Rajeswara Palanichamy).

framework of density functional theory and the Full Potential Linearly Augmented Plane Wave (FP-LAPW) [34] technique to examine the structural, electronic, magnetic, and thermoelectric properties of the ZrCoSb and Fe substituted ZrCoSb half-Heusler alloys. In order to investigate the exchange-correlation effects within the scheme of the Generalised Gradient Approximation (GGA) technique, we employed the Perdew–Burke–Ernzerhof exchange-correlation functional [35,36]. The Kohn-Sham equations [37] are employed for the use of calculating the density of both majority and minority spin states. A 12-atom supercell, which is equivalent to a $1 \times 1 \times 1$ conventional cubic cell,

is employed so as to simulate various substitution concentrations. We used Cut-off energy of -6 Ry, L_{\max} of 10, RK_{\max} of 8, and G_{\max} of 12. The core states were treated relativistically, while the semi-core states were treated semi-relativistically, ignoring the spin-orbit (SO) coupling. The k integration over the Brillouin zone in the irreducible Brillouin Zone is performed with a $(15 \times 15 \times 15)$ grid. The charge and energy convergence conditions are 0.0001 e and 0.00001 Ry, respectively. Constant hydrostatic pressure is applied in all directions to compute elastic properties using the cubic elastic code [38]. The semi-classical Boltzmann transport theory, as defined in the BoltzTraP2 algorithm [39], is

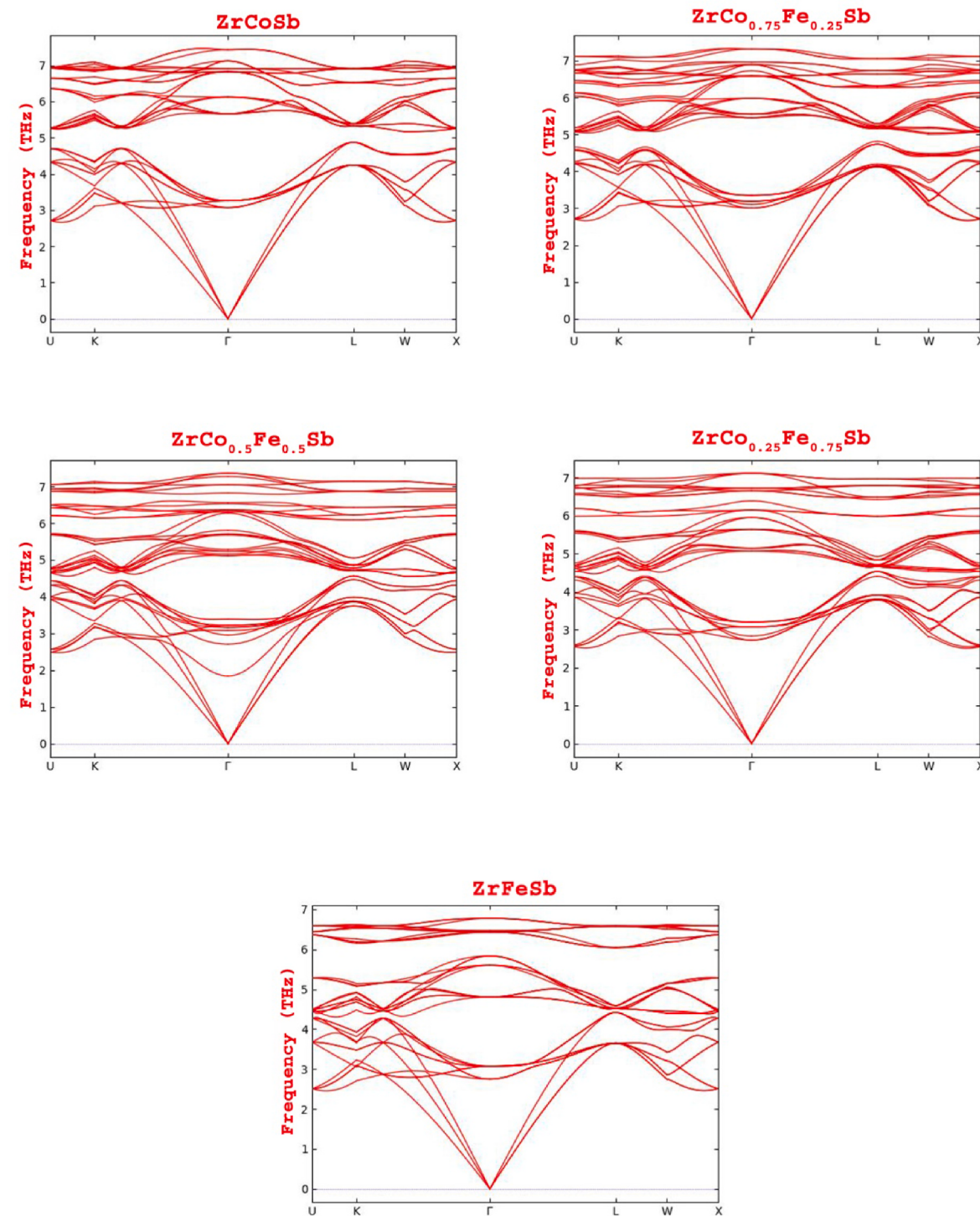


Fig. 1. Phonon dispersion curves of $ZrCo_{1-x}Fe_xSb$ ($X = 0, 0.25, 0.5, 0.75, 1$).

used to estimate thermoelectric properties using the constant relaxation time and rigid band approximations.

3. Results and discussion

In this study, we examined the characteristics of half-Heusler alloys $ZrCo_{1-x}Fe_xSb$, where X represents the varying compositions of 0, 0.25, 0.5, 0.75, and 1. The valence state electrons of Zirconium (Zr), Cobalt (Co), Iron (Fe), and Antimony (Sb) are considered to be $4d^25s^2$, $3d^74s^2$, $3d^64s^2$, and $5s^25p^3$, respectively, in the calculation.

3.1. Structural stability

The crystal structure of half-Heusler alloys, namely the non-centrosymmetric cubic ($C1_b$) structure, is characterised by the presence of three interpenetrating face-centered cubic (fcc) lattices. The crystal structure is classified under the $F43m$ space group. The atoms in these alloys are located in the Wyckoff positions: Zr atom at 4 b ($1/2, 1/2, 1/2$), Co or Fe atom at 4c ($1/4, 1/4, 1/4$), and Sb atom at 4a (0, 0, 0). Computational investigations on $ZrCo_{1-x}Fe_xSb$ ($X = 0, 0.25, 0.5, 0.75, 1$) alloys with varied compositions are performed to determine the lattice parameter.

Birch-Murnaghan's empirical equation [40,41] is used to calculate ground state characteristics such as the lattice constant a_0 , the bulk modulus B, and its first derivative B' by fitting the estimated total energy against the equilibrium volume. The structural optimisation of $ZrCoSb$ is first carried out, and it found to be stable in the cubic non-magnetic semiconducting phase with a lattice constant of 6.0973 \AA . This lattice constant value is consistent with Ref. [21]. The $ZrCo_{1-x}Fe_xSb$ ($X = 0.25, 0.5, 0.75, 1$) alloys exhibit a crystalline structure in the cubic ferromagnetic phase. The lattice constant predicted for $ZrFeSb$ matches with the results obtained by Özdemir EG and Merdan Z.

The phonon dispersion curve generated by the PHONOPY package [42] is used to investigate the structural stability of $ZrCo_{1-x}Fe_xSb$ ($X = 0, 0.25, 0.5, 0.75, 1$) alloys. The phonon computations for the $ZrCo_{1-x}Fe_xSb$ ($X = 0, 0.25, 0.5, 0.75, 1$) alloy in the cubic $C1_b$ structure are performed using the supercell finite-displacement method. Wien2K serves as the force constant calculator. Fig. 1 shows the phonon dispersion band curves for $ZrCo_{1-x}Fe_xSb$ ($X = 0, 0.25, 0.5, 0.75, 1$) alloys. The generated phonon dispersion curves for $ZrCo_{1-x}Fe_xSb$ ($X = 0, 0.25, 0.5, 0.75, 1$) alloys exhibit no negative frequencies, showing that all of these alloys are stable in the cubic $C1_b$ structure.

The formation energy can also be used to find the stability of the $ZrCo_{1-x}Fe_xSb$ ($X = 0, 0.25, 0.5, 0.75, 1$) alloys. The formation energy of a material can be determined using the following formula:

$$E_f = E_{ZrCo_{1-x}Fe_xSb} - n_{Zr}E_{Zr} - n_{Co}E_{Co} - n_{Fe}E_{Fe} - n_{Sb}E_{Sb}$$

where, n_{Zr} , n_{Co} , n_{Fe} and n_{Sb} are number of Zr, Co, Fe and Sb atoms in $ZrCo_{1-x}Fe_xSb$ unit cell, respectively. The alloys $ZrCo_{1-x}Fe_xSb$ ($X = 0, 0.25, 0.5, 0.75, 1$) exhibit negative formation energies. This suggests that these alloys have the capability to be easily produced at room

temperature. The computed structural parameters such as lattice constant (a_0), equilibrium volume (V_0), total energy (E), formation energy (E_f), bulk modulus (B), and its derivative (B') for the alloys $ZrCo_{1-x}Fe_xSb$ ($X = 0, 0.25, 0.5, 0.75, 1$) are presented in Table 1.

3.2. Mechanical stability

The materials elastic properties are important for analysing its mechanical stability, making them useful for a variety of practical applications. The IRelast package, which is integrated with the Wien2k code, is used to compute the elastic constants and elasticity moduli of a cubic crystal. The structural strength of a cubic crystal system is determined by three unique elastic constants (C_{11} , C_{12} , and C_{14}). C_{11} refers to material strain resistance, C_{12} to shear stress, and C_{14} to shear deformation resistance. In order to assess the stability of alloys, the Born-Huang criterion ($C_{11} - C_{12} > 0$, $(C_{11} + 2C_{12}) > 0$, $C_{11} > 0$, $C_{44} > 0$, $C_{12} < B < C_{11}$) is used in the investigation of mechanical properties [43,44]. The calculated elastic constants, elastic moduli, Poisson's ratio, Cauchy's pressure, anisotropy factor, Debye temperature, and melting temperature for $ZrCo_{1-x}Fe_xSb$ alloys are shown in Tables 2 and 3. Table 2 provides evidence that the $ZrCo_{1-x}Fe_xSb$ half Heusler alloys satisfy the stability criteria for elastic constants, hence confirming their mechanical stability.

The $ZrCo_{1-x}Fe_xSb$ half Heusler alloys exhibit a notable characteristic of high bulk modulus, rendering them effectively incompressible. The bulk moduli for $ZrCoSb$, $ZrCo_{0.75}Fe_{0.25}Sb$, $ZrCo_{0.5}Fe_{0.5}Sb$, $ZrCo_{0.25}Fe_{0.75}Sb$ and $ZrFeSb$ are 140.18 GPa , 130.445 GPa , 128.118 GPa , 122.604 GPa , and 121.343 GPa , respectively. These results are similar to those found using Birch-Murnaghan's equation of state (135.748 GPa , 131.999 GPa , 128.726 GPa , 120.246 GPa , and 119.665 GPa , respectively). The high bulk modulus of all these alloys causes incompressibility and high bond strength. The shear modulus exhibits resistance to deformations caused by shear stress, and the determination of the shear modulus for $ZrCo_{1-x}Fe_xSb$ half Heusler alloys provides valuable insight into the directional bonding interactions among the constituent atoms, which has considerable importance. Young's modulus is a fundamental property used to quantify the rigidity of a solid. It determines a material's resistance to deformation under applied stress. The value of Young's modulus indicates that $ZrCo_{1-x}Fe_xSb$ is a rigid material. A low B/G value denotes brittleness, whereas a high value implies ductility. The material behaviour is distinguished by the G/B value. If G/B is less than 0.5, the material is brittle, and if G/B is greater than 0.5, the material is ductile [45–47]. According to the calculated B/G and G/B values, all of these $ZrCo_{1-x}Fe_xSb$ ($X = 0, 0.25, 0.5, 0.75, 1$) alloys are ductile. The Cauchy's pressure value $CP = C_{12} - C_{44}$ is positive, indicating that the materials are ductile [48]. The anisotropy factor (A) indicates whether a crystal is anisotropic or isotropic [49–51]. A = 1 represents an isotropic crystal, while $A < 1$ or $A > 1$ represents an anisotropic crystal. These $ZrCo_{1-x}Fe_xSb$ ($X = 0, 0.25, 0.5, 0.75, 1$) alloys are anisotropic because the coefficient A is less than one.

Table 1

Calculated lattice parameter $a_0(\text{\AA})$, equilibrium volume $V_0 (\text{\AA}^3)$, total energy $E_{\text{Tot}}(\text{Ry})$, formation energy $E_f(\text{Ry})$, bulk modulus B (GPa) and its derivative B' for $ZrCo_{1-x}Fe_xSb$ ($X = 0, 0.25, 0.5, 0.75, 1$).

Compound	a_0	V_0	E_{Tot}	E_f	B	B'
$ZrCoSb$	6.0973 6.0912 ^a	382.445	-22952.777	-1.228	135.748	4.565
$ZrCo_{0.75}Fe_{0.25}Sb$	6.1188	1545.987	-91569.693	-4.699	131.999	4.306
$ZrCo_{0.5}Fe_{0.5}Sb$	6.1389	1561.229	-91328.270	-4.677	128.726	4.097
$ZrCo_{0.25}Fe_{0.75}Sb$	6.1523	1571.486	-91086.865	-4.672	120.246	3.947
$ZrFeSb$	6.1701 6.172 ^b	396.286	-22711.412	-1.214	119.665 120.836 ^b	4.405

^a Ref. [21] Theo.

^b Ref. [23] Theo.

Table 2

Calculated elastic constants C_{ij} (GPa), Voigt – Reuss – Hill bulk modulus B (GPa), shear modulus G (GPa), B/G ratio, G/B ratio, and Young's modulus E (GPa), of $ZrCo_{1-x}Fe_xSb$ ($X = 0, 0.25, 0.5, 0.75, 1$).

Compound	C_{11} (GPa)	C_{12} (GPa)	C_{44} (GPa)	B(GPa)	G(GPa)	B/G	G/B	E(GPa)
$ZrCoSb$	269.866	75.339	74.55	140.18	82.231	1.704	0.587	207.816
	263.0 ^a	78.1 ^a	71.7 ^a	139.78 ^a	79.39 ^a			202.03 ^a
$ZrCo_{0.75}Fe_{0.25}Sb$	248.964	71.186	67.025	130.445	75.054	1.738	0.575	188.927
$ZrCo_{0.5}Fe_{0.5}Sb$	239.314	72.52	68.386	128.118	74.041	1.73	0.577	186.982
$ZrCo_{0.25}Fe_{0.75}Sb$	222.313	72.750	65.984	122.604	69.372	1.767	0.565	175.092
$ZrFeSb$	220.611	71.710	70.673	121.343	72.16	1.705	0.586	180.667
	198.739 ^b	77.927 ^b	61.098 ^b	118.198 ^b	60.821 ^b			155.748 ^b

^a Ref. [21] Theo.

^b Ref. [23] Theo.

^c Ref. [20] Expt.

Table 3

Calculated Poisson's ratio ν , Cauchy pressure (GPa), anisotropy factor A, Debye temperature θ_D (K) and melting temperature T_m (K) of $ZrCo_{1-x}Fe_xSb$ ($X = 0, 0.25, 0.5, 0.75, 1$).

Compound	ν	CP(GPa)	A	θ_D (K)	T_m (K)
$ZrCoSb$	0.252	0.789	0.766	400.335	2147.912
	0.25 ^a		0.76 ^a	392.073 ^a	
				399 ^c	
				392 ^d	
$ZrCo_{0.75}Fe_{0.25}Sb$	0.258	4.161	0.754	382.562	2024.380
$ZrCo_{0.5}Fe_{0.5}Sb$	0.257	4.133	0.82	375.528	1967.346
$ZrCo_{0.25}Fe_{0.75}Sb$	0.261	6.765	0.882	369.953	1866.871
$ZrFeSb$	0.251	1.036	0.949	377.945	1856.810
	0.280 ^b				

^a Ref. [21] Theo.

^b Ref. [23] Theo.

^c Ref. [20] Expt.

^d Ref. [22] Expt.

3.3. Electronic properties

Using spin-polarized calculations, the electronic structure of $ZrCo_{1-x}Fe_xSb$ ($X = 0, 0.25, 0.5, 0.75, 1$) half Heusler alloys has been studied. GGA-Perdew-Burke-Ernzerhof (PBE) and Tran–Blaha modified Becke–Johnson exchange potential approximation (TB-mBJ) techniques are used to calculate the band structure of $ZrCo_{1-x}Fe_xSb$ ($X = 0, 0.25, 0.5, 0.75, 1$) half Heusler alloys. The band gaps calculated by the GGA and TB-mBJ techniques are slightly different. Fig. 2 shows the spin-polarized band structures computed for $ZrCo_{1-x}Fe_xSb$ alloys along high symmetry directions in the first Brillouin zone using GGA technique, and the calculated band gap values are listed in Table 4. The band structure for the TB-mBJ technique is not shown as all of these alloys exhibit the same band structure characteristics as the GGA technique. The horizontal red dashed lines represent the Fermi level E_F , which is set at zero energy. The semiconducting nature of the $ZrCoSb$ alloy with a 1.077 eV band gap is shown in Fig. 2. This gap between the d-states of Zr and Co and the p-state of Sb in the VBM (CBM) appears at the L (X) high-symmetry lines of the d-states of Zr and Co in the conduction band. The calculated band gap value of $ZrCoSb$ is consistent with the other findings [20,21]. For all Fe concentrations, a gap is observed in the spin up state, indicating semiconductor-like characteristics, however there is no gap below the Fermi level E_F , confirming that the spin down state has a metallic character, suggesting that these alloys are half-metallic.

Consequently, using the PBE-GGA approximation, the partial density of states (PDOS) and total density of states (TDOS) are computed at normal pressure and presented in Fig. 3, illustrates the electronic properties of the $ZrCo_{1-x}Fe_xSb$ ($X = 0, 0.25, 0.5, 0.75, 1$) half Heusler alloys under study. A vertical dash line represents the Fermi level, which is set at zero energy. The $ZrCo_{1-x}Fe_xSb$ ($X = 0.25, 0.5, 0.75, 1$) alloys exhibit a semiconducting property in the spin-up state. There is an

observable hybridization between the d orbitals of Zr, Fe, and Co atoms, and it is clear that the peaks of their d states cross the Fermi level. Thus, in the spin-down state, the material under study shows metallic characteristics. The dstates of Zr, Fe, and Co atoms dominate the valence band top and the conduction band bottom, with a small contribution from Sb-p states. Additionally, as seen in Fig. 3, we find two regions in the valence bands. The Sb-p states dominate the first region at -5.2 and -2.5 eV. The second region, between -1.9 and -0.25 eV, is dominated by the d states of Zr, Fe and Co atoms with weak hybridization of Sb-p states. It is certain that the observed peaks in the conduction bands are mostly caused by the d states of Zr, Fe and Co atoms, with a minor contribution from the Sb-pstates. The DOS appears to change significantly when a Fe atom is substituted. The spin-down states of $ZrCo_{0.75}Fe_{0.25}Sb$, $ZrCo_{0.5}Fe_{0.5}Sb$, and $ZrCo_{0.25}Fe_{0.75}Sb$ show their metallic character noticeable. In the spin-up states, the corresponding energy gaps (E_g) are measured to be 1.054, 1.028, and 1.001 eV, respectively. As a consequence, the energy gap values drop when the Co atom is replaced with the Fe atom. The transition metal atom Fe is primarily responsible for determining whether there is a half-metallic gap in the vicinity of the Fermi level. The observed gap is localised within the d-states of Zr and Co/Fe atoms, as well as the p-state of Sb atom. The presence of hybridization of d states of Zr, Fe, and Co atoms is responsible for the formation of gap in the spin-up state. It reveals that the substitution of Fe in $ZrCoSb$ results in a decrease in the number of valence electrons. Furthermore, the substitution causes a shift of the electronic states of the constituent atoms in the $ZrCoSb$ alloy to lower energy levels. Significant changes in the electronic structure of the $ZrCoSb$ alloy are caused by the substitution of a Fe atom at the Co atom position. The change is caused by the proximity of -dstate electrons of a Fe atom hybridised with a Co atom. The spin-down state of $ZrFeSb$ has no energy gap, but the spin-up state has a gap of 0.967 eV, indicating that it is half metallic. It agrees with the previous result [23].

In this study, we employ spin-polarized computations to examine the electronic characteristics of $ZrCo_{1-x}Fe_xSb$ half Heusler alloys, with the aim of investigating their possible applications in the field of spintronics. The following equation is used to determine the electron spin-polarisation at the Fermi level [52].

$$P = \frac{\rho \uparrow(E_F) - \rho \downarrow(E_F)}{\rho \uparrow(E_F) + \rho \downarrow(E_F)}$$

where $\rho \uparrow(E_F)$ denotes the spin dependent density of spin-up state and $\rho \downarrow(E_F)$ denotes the spin dependent density of spin-down state. The percentage of spin polarisation for $ZrCo_{1-x}Fe_xSb$ alloys has been estimated using the formula above. At normal pressure, the investigated half Heusler alloys $ZrCo_{0.75}Fe_{0.25}Sb$, $ZrCo_{0.5}Fe_{0.5}Sb$, $ZrCo_{0.25}Fe_{0.75}Sb$ and $ZrFeSb$ are half metals. The polarisation of $ZrCo_{1-x}Fe_xSb$ half Heusler alloy increases with Fe concentration and is calculated to be equal to 93.5, 99.9, 100, and 100 % respectively, at concentration $X = 25, 50, 75$, and 100 %. The $ZrCo_{0.25}Fe_{0.75}Sb$ and $ZrFeSb$ alloys have 100 % polarisation and hence satisfy the half-metallic property.

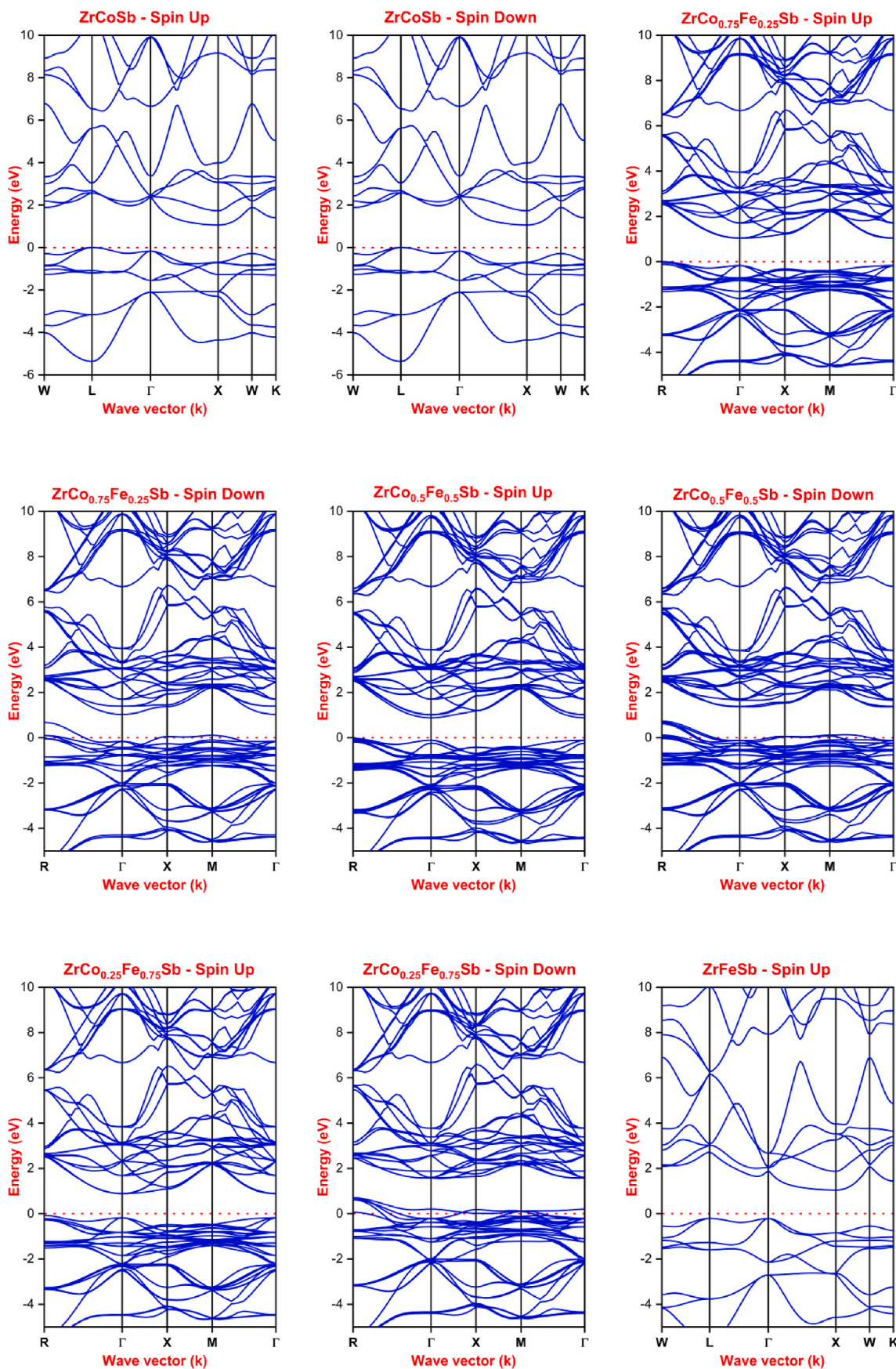


Fig. 2. The electronic band structure of $\text{ZrCo}_{1-x}\text{Fe}_x\text{Sb}$ ($X = 0, 0.25, 0.5, 0.75, 1$).

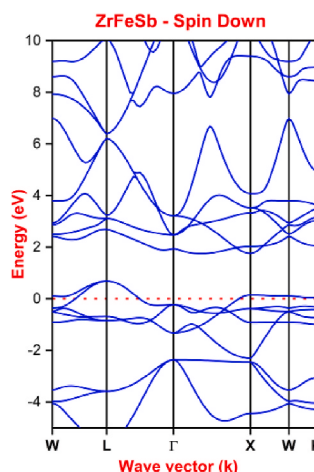


Fig. 2. (continued).

Table 4
Calculated band gap energy E_g (eV) of $ZrCo_{1-x}Fe_xSb$ ($X = 0, 0.25, 0.5, 0.75, 1$).

Compound	E_g (eV)	
	GGA	TB-mBJ
$ZrCoSb$	1.077	1.144
	1.073 ^a	
$ZrCo_{0.75}Fe_{0.25}Sb$	1.054	1.090
$ZrCo_{0.5}Fe_{0.5}Sb$	1.028	1.071
$ZrCo_{0.25}Fe_{0.75}Sb$	1.001	1.045
$ZrFeSb$	0.967	0.849
	0.96 ^b	0.84 ^b

^a Ref. [21] Theo.

^b Ref. [23] Theo.

3.4. Magnetic properties

The magnetic moments of $ZrCo_{1-x}Fe_xSb$ ($X = 0, 0.25, 0.5, 0.75, 1$) are provided in Table 5, including the total and interstitial spin magnetic moments. The Slater-Pauling rule [53,54] has been demonstrated to establish a direct relationship between the total magnetic moment (M_T) and the total number of valence electrons (Z_T) while investigating the half-metallic property.

$$M_T = Z_T - 18 \quad 18$$

The magnetic moment values of $ZrCoSb$ ($0 \mu\text{B}$) and $ZrFeSb$ ($1 \mu\text{B}$) are observed to conform the Slater-Pauling rule. Furthermore, the substitution of Fe into the $ZrCoSb$ alloy increases magnetism in the resulting $ZrCo_{0.75}Fe_{0.25}Sb$, $ZrCo_{0.5}Fe_{0.5}Sb$, and $ZrCo_{0.25}Fe_{0.75}Sb$ alloys. The magnetic moment of $ZrCo_{1-x}Fe_xSb$ increases from 0 to $1 \mu\text{B}$ as X increased from 0 to 1 . Thus, the substitution of Fe enhances the magnetic properties of $ZrCoSb$. The magnetic moments of Co and Fe are paired ferromagnetically in the $ZrCo_{1-x}Fe_xSb$ ($X = 0, 0.25, 0.5, 0.75, 1$) alloys.

3.5. Thermoelectric properties

The Boltzmann transport theory, as implemented in the BoltzTraP2 method with constant relaxation time and rigid band approximations, is used to analyse thermoelectric properties. The GGA technique is used to compute the Seebeck coefficient, electrical and thermal conductivities, and power factor in the spin up state of $ZrCo_{1-x}Fe_xSb$ alloys. An essential thermoelectric parameter utilised for predicting the thermoelectric capabilities of materials is the Seebeck coefficient, which establishes a relationship between thermal and electrical conductivity. The predicted thermoelectric characteristics of $ZrCo_{1-x}Fe_xSb$ alloys for spin up state are shown as a function of temperature.

Fig. 4 displays the temperature dependence of the Seebeck coefficients for $ZrCo_{1-x}Fe_xSb$ alloys. The $ZrCo_{1-x}Fe_xSb$ alloy possesses a positive Seebeck coefficient over the entire predicted temperature range when X is increased from 0 to 1 . The Seebeck coefficient for $ZrCoSb$, $ZrCo_{0.75}Fe_{0.25}Sb$, $ZrCo_{0.5}Fe_{0.5}Sb$, and $ZrCo_{0.25}Fe_{0.75}Sb$ alloys rises with temperature up to 800 K before dropping out. $ZrCoSb$, $ZrCo_{0.75}Fe_{0.25}Sb$, $ZrCo_{0.5}Fe_{0.5}Sb$, and $ZrCo_{0.25}Fe_{0.75}Sb$ all have maximum Seebeck coefficients at 800 K, with values of 197.7 , 195.1 , 190.8 , and $293.4 \mu\text{V/K}$, respectively. The Seebeck coefficient value of $ZrCoSb$ agrees with that found in Refs. [19,20]. At 100 K, $ZrFeSb$ has a maximum Seebeck coefficient of around $1068.7 \mu\text{V/K}$. The Seebeck coefficient for $ZrFeSb$ drops as the temperature rises.

Fig. 5 depicts the relationship between electrical conductivity (σ/τ) and temperature. However, the value of electrical conductivity increases with temperature, but pure $ZrCoSb$ exhibits the maximum value of electrical conductivity of $0.53 \times 10^{19}/\Omega\text{m}$ at 1100 K. The fact that electrical conductivity in the spin up state rises linearly with increasing temperature supports the band structure, confirming the semiconducting characteristic. Fig. 6 depicts the electronic thermal conductivity (κ/τ) as a function of temperature around the Fermi level. As the temperature rises, the electronic thermal conductivity of the spin up state increases.

The power factor (PF) is a measure of the efficiency of a material in thermoelectric applications. It can be calculated using the Seebeck coefficient and electrical conductivity ($\text{PF} = S^2\sigma/\tau$). Fig. 7 depicts the power factor of $ZrCo_{1-x}Fe_xSb$ alloys as a function of temperature. All of these alloys show an increase in power factor as temperature rises. Materials having a high value are considered to be more advantageous for thermoelectric applications, where the power factor should be unity or greater [55]. The values of $S^2\sigma/\tau$ for $ZrCoSb$, $ZrCo_{0.75}Fe_{0.25}Sb$, $ZrCo_{0.5}Fe_{0.5}Sb$, $ZrCo_{0.25}Fe_{0.75}Sb$ and $ZrFeSb$ at room temperature are $1.58 \times 10^{11} \text{ W/mks}$, $1.84 \times 10^{11} \text{ W/mks}$, $8.39 \times 10^{10} \text{ W/mks}$, $1.54 \times 10^{10} \text{ W/mks}$, and $4.88 \times 10^9 \text{ W/mks}$, respectively. These high values show these alloys will be effective thermoelectric materials.

4. Conclusion

Using first-principles calculation, we predicted the structural, electronic, magnetic, and thermoelectric properties of the half-Heusler alloys $ZrCo_{1-x}Fe_xSb$ ($X = 0, 0.25, 0.5, 0.75, 1$). The real phonon frequency value reveals that the $ZrCo_{1-x}Fe_xSb$ alloy is structurally stable. Elastically, the required mechanical stability criteria are met, and thus $ZrCo_{1-x}Fe_xSb$ ($X = 0, 0.25, 0.5, 0.75, 1$) alloys are found to be ductile and anisotropic materials. The density of states and band structure plot assures the semiconducting behaviour for $ZrCoSb$ and half-metallic behaviour for $ZrFeSb$. When Fe is substituted for Co in $ZrCoSb$, the

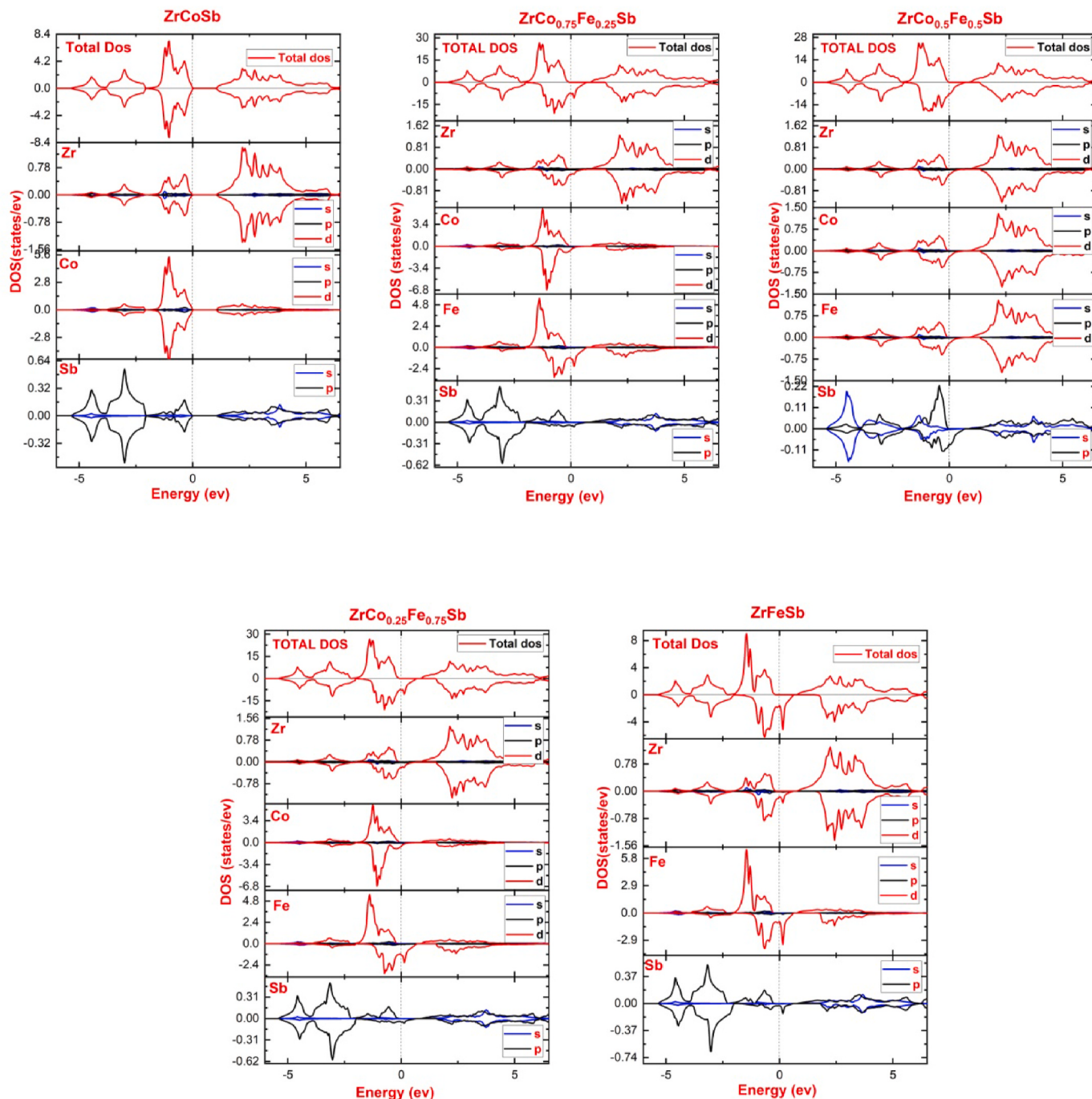


Fig. 3. Total density of states (DOS) and Partial density of states (PDOS) of $ZrCo_{1-X}Fe_XSb$ ($X = 0, 0.25, 0.5, 0.75, 1$) at normal pressure.

Table 5

Calculated total magnetic moment (μ_{Tot} in μ_B) per unit cell and the local magnetic moment of each site $ZrCo_{1-X}Fe_XSb$ ($X = 0, 0.25, 0.5, 0.75, 1$).

Compound	μ_{int}	μ_{Zr}	μ_{Co}	μ_{Fe}	μ_{Sb}	μ_{Tot}
ZrCoSb	0	0	0	–	0	0
ZrCo _{0.75} Fe _{0.25} Sb	0.00687	-0.00362	0.00241	0.26132	0.00205	0.26904
ZrCo _{0.5} Fe _{0.5} Sb	0.00363	-0.019465	0.01218	0.54375	0.00274	0.49665
ZrCo _{0.25} Fe _{0.75} Sb	-0.00884	-0.02612	0.02758	0.57832	0.00203	0.57298
ZrFeSb	-0.05936	-0.15592	–	1.20199	0.00834	0.99505
		-0.162 ^a		1.219 ^a	0.0085 ^a	1.0 ^a

^a Ref. [23] Theo.

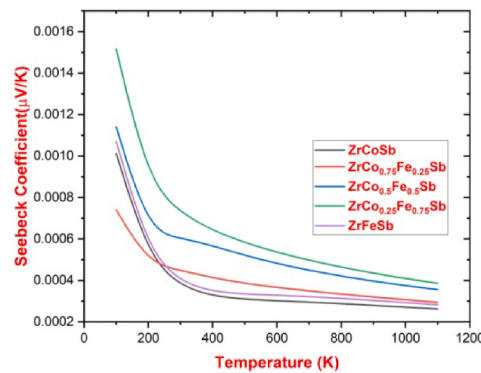


Fig. 4. The variation of Seebeck coefficient (S) with temperature of $\text{ZrCo}_{1-x}\text{Fe}_x\text{Sb}$ ($X = 0, 0.25, 0.5, 0.75, 1$).

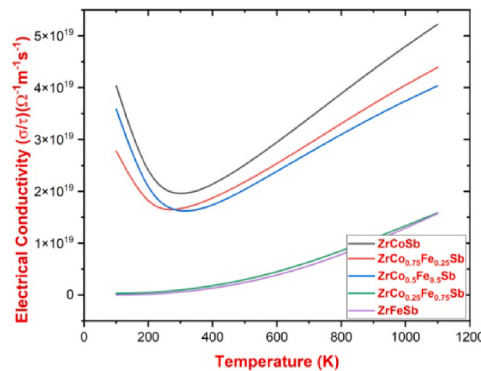


Fig. 5. The variation of electrical conductivity (σ/τ) with temperature of $\text{ZrCo}_{1-x}\text{Fe}_x\text{Sb}$ ($X = 0, 0.25, 0.5, 0.75, 1$).

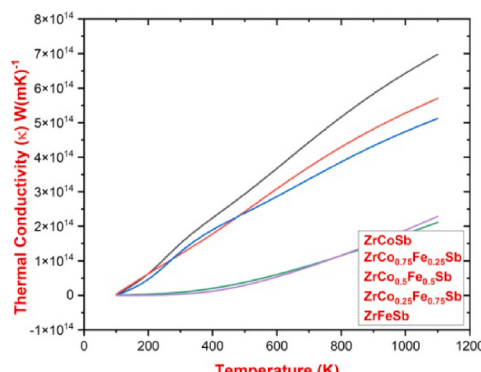


Fig. 6. The variation of thermal conductivity with temperature of $\text{ZrCo}_{1-x}\text{Fe}_x\text{Sb}$ ($X = 0, 0.25, 0.5, 0.75, 1$).

resulting alloys $\text{ZrCo}_{0.75}\text{Fe}_{0.25}\text{Sb}$, $\text{ZrCo}_{0.5}\text{Fe}_{0.5}\text{Sb}$, and $\text{ZrCo}_{0.25}\text{Fe}_{0.75}\text{Sb}$ are half metallic. ZrCoSb is non-magnetic, however, $\text{ZrCo}_{0.75}\text{Fe}_{0.25}\text{Sb}$, $\text{ZrCo}_{0.5}\text{Fe}_{0.5}\text{Sb}$, $\text{ZrCo}_{0.25}\text{Fe}_{0.75}\text{Sb}$ and ZrFeSb are ferromagnetic, based on spin polarised calculations. The total magnetic moment values of these alloys satisfy the Slater-Pauling (SP) rule. For the spin up state, the relationship between thermoelectric properties and temperature of $\text{ZrCo}_{1-x}\text{Fe}_x\text{Sb}$ ($X = 0, 0.25, 0.5, 0.75, 1$) alloys has been established. The overall characteristics of the material indicate that it is suitable for thermoelectric and spintronic applications.

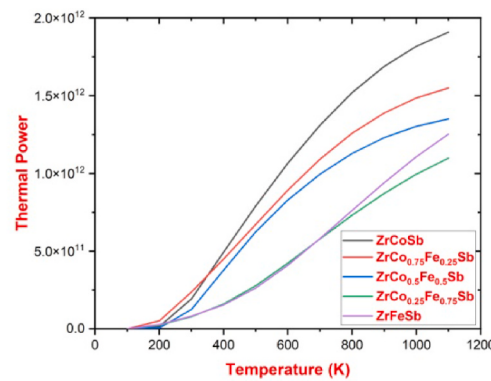


Fig. 7. The variation of power factor with temperature of $\text{ZrCo}_{1-x}\text{Fe}_x\text{Sb}$ ($X = 0, 0.25, 0.5, 0.75, 1$).

CRediT authorship contribution statement

R. Meenakshi: Writing – original draft, Data curation. R. Aram Senthil Srinivasan: Software, Investigation. A. Amudhavalli: Validation, Methodology. K. Iyakutti: Writing – review & editing, Supervision. Y. Kawazoe: Supervision, Investigation. R. Rajeswara Palanichamy: Writing – review & editing.

Declaration of competing interest

The authors declare that they have no known competing financial interests or personal relationships that could have appeared to influence the work reported in this paper.

Data availability

The data that has been used is confidential.

Acknowledgement

The support received from the college management is duly acknowledged with gratitude. The authors are grateful to Professor Blaha for providing Wien2K software.

Author KI acknowledges supercomputing resources from the Center for Computational Materials Science of the Institute for Materials Research, Tohoku University and SRM Institute of Science and Technology.

References

- [1] F. Heusler, W. Starck, E. Haupt, Magnetic chemical studies, *Verhandlungen Dtsch. Phys. Ges.* 5 (1903) 219–232.
- [2] C. Felser, G.H. Fecher, *Spintronics: from Materials to Devices*, Springer, Netherlands, 2013.
- [3] K.H.J. Buschow, and P.G. van Engen, Magnetic and magneto optical properties of Heusler alloys based on aluminium and gallium, *J. Magn. Magn Mater.* 25 (1) (1981) 90–96.
- [4] C. Palmström, Epitaxial heusler alloys: new materials for semiconductor spintronics, *MRS Bull.* 28 (2003) 725–728.
- [5] A. Hirohata, J. Sagar, L. Lari, L.R. Fleet, V.K. Lazarov, Heusler-alloy films for spintronic devices, *Appl. Phys. A* 111 (2013) 423–430.
- [6] Z. Wen, T. Kubota and K. Takanashi, Optimization of half Heusler PtMnSb alloy films for spintronic device applications, *J. Phys. D Appl. Phys.* 51 (43) (2018) 435002.
- [7] M. Belkhouane, S. Amari, A. Yakoubi, A. Tadjer, S. Méçabih, G. Murtaza, S. B. Omran, R. Khenata, First-principles study of the electronic and magnetic properties of Fe_2MnAl , Fe_2MnSi and $\text{Fe}_2\text{MnSi}0.5\text{Al}0.5$, *J. Magn. Magn Mater.* 377 (1) (2015) 211–214.
- [8] I. Galanakis, K. Özdogan, E. Şaşıoğlu, Spin-filter and spin-gapless semiconductors: the case of Heusler compounds, *AIP Adv.* 6 (2016) 055606.
- [9] Z. Wen, H. Sukegawa, S. Kasai, K. Inomata, S. Mitani, Tunnel magnetoresistance and spin-transfer-torque switching in polycrystalline Co_2FeAl full-Heusler Alloy magnetic tunnel junctions on amorphous Si/SiO_2 substrates, *Phys. Rev. Appl.* 2 (2014) 024009.

- [10] T. Tsuchiya, T. Roy, K. Elphick, J. Okabayashi, L. Bainsla, T. Ichinose, K.Z. Suzuki, M. Tsujikawa, M. Shirai, A. Hirohata, S. Mizukami, Magnetic tunnel junctions with a B2-ordered CoFeCrAlHeusler alloy, *Phys. Rev. Mater.* 3 (2019) 084403.
- [11] S. Bhatti, R. Sbiaa, A. Hirohata, H. Ohno, S. Fukami, S.N. Piramanayagam, Spintronics based random access memory: a review, *Mater. Today* 20 (9) (2017) 530–548.
- [12] J. Winterlik, G.H. Fecher, A. Thomas and C. Felser, Superconductivity in palladium based Heusler compounds, *Phys. Rev. B* 79 (2009) 064508.
- [13] J. Schmitt, Z. Gibbs, G. Schnyder, G. C. Felser, Resolving the true band gap of $ZrNiSn$ half-Heusler thermoelectric materials, *Mater. Horiz.* 2 (2014) 68–75.
- [14] A. Page, A. van der Ven, P.F.P. Poudeau and C. Uher, Origins of phase separation in thermoelectric (Ti, Zr, Hf) NiSn half-Heusler alloys from first principles, *J. Mater. Chem. A* 4 (2016) 13949–13956.
- [15] M. Zhang, J. Wei and G. Wang, Thermoelectric and topological properties of half-Heusler compounds $ZrIrX$ (As, Sb, Bi), *Phys. Lett.* 382 (9) (2018) 673–678.
- [16] R.J. Quinn, J.W.G. Bos, Advances in half-Heusler alloys for thermoelectric power generation, *Mater. Adv.* 2 (2021) 6246–6266.
- [17] W.G. Zeier, J. Schmitt, G. Hautier, U. Aydemir, Z.M. Gibbs, C. Felser, G.J. Snyder, Engineering half-Heusler thermoelectric materials using Zintl chemistry, *Nat. Rev. Mater.* 1 (6) (2016) 16032.
- [18] J. Tobola, J. Pierre, Electronic phasediagram of the X TZ (X =Fe, Co, Ni; T =Ti, V, Zr, Nb, Mn; Z =Sn, Sb) semi-Heusler compounds, *J. Alloys Compd.* 296 (2000) 243–252.
- [19] Y. Xia, S. Bhattacharya, V. Ponnambalam, A.L. Pope, S.J. Poon, and T.M. Tritt, Thermoelectric properties of semimetallic (Zr, Hf)CoSb half-Heusler phases, *J. Appl. Phys.* 88 (2000) 1952–1955.
- [20] T. Sekimoto, K. Kurosaki, H. Muta, S. Yamanaka, Thermoelectric and thermophysical properties of $TiCoSb$ - $ZrCoSb$ - $HfCoSb$ prepared by spark plasma sintering, *Mater. Trans.* 47 (6) (2006) 1445–1448.
- [21] H. Joshi, D.P. Rai, L. Hnamte, A. Larefand, R.K. Thapa, A theoretical analysis of elastic and optical properties of half Heusler $MCoSb$ (M =Ti, Zr and Hf), *Heliyon* 5 (3) (2019) e01155.
- [22] S. Li, H. Zhao, D. Li, S. Jin, L. Gu, Synthesis and thermoelectric properties of half-Heusler alloy $YNiBi$, *J. Appl. Phys.* 117 (2015) 205101.
- [23] E.G. Özdemir, Z. Merdan, Theoretical calculations on half-metallic results properties of $FeZrX$ (X = P, As, Sb and Bi) half-Heusler compounds: density Functional Theory, *Mater. Res. Express* 6 (2019) 086102.
- [24] E. Rausch, B. Balke, S. Ouardi, C. Felser, Long-term stability of (Ti/Zr/Hf) $CoSb_{1-x}Sn_x$ thermoelectric p-type half-Heusler compounds upon thermal cycling, *Energ. Tech.* 3 (2015) 1217.
- [25] V. Ponnambalam, P.N. Alboni, J. Edwards, T.M. Tritt, S.R. Culp, S.J. Poon, Thermoelectric properties of p-type half-Heusler alloys $Zr_{1-x}Ti_xCoSn_{y}Sb_{1-y}$ ($0.0 < x < 0.5$; $y = 0.15$ and 0.3), *J. Appl. Phys.* 103 (2008) 063716.
- [26] T. Wu, W. Jiang, X. Li, Y. Zhou, L. Chen, Thermoelectric properties of p-type Fe doped $TiCoSb$ half-Heusler compounds, *J. Appl. Phys.* 102 (2007) 103705–103711.
- [27] G. Melnyk, E. Bauer, P. Rogl, R. Skolozdra, E. Seidl, Thermoelectric properties of ternary transition metal antimonides, *J. Alloys Compd.* 296 (2000) 235–242.
- [28] P. Maji, N.J. Takas, D.K. Misra, H. Gabrisch, K. Stokes, P.F.P. Poudeu, Effects of Rh on the thermoelectric performance of the p-type $Zr_{0.5}Hf_{0.5}Co_{1-x}Rh_xSb_{0.99}Sn_{0.01}$ half-Heusler alloys, *J. Solid State Chem.* 183 (2010) 1120–1126.
- [29] N.J. Takas, M.R. Shabetai, P.F.P. Poudeu, Effect of Sn doping on the thermoelectric performance of the complex p-type $Zr0.5Hf0.5Co0.3Ir0.7Sb1-ySn_y$ half-heusler system, *Sci. Adv. Mater.* 3 (2011) 571–576.
- [30] N.S. Chauhan, A. Bhardwaj, T. Senguttuvan, R. Pant, R. Mallik, D.K. Misra, A synergistic combination of atomic scale structural engineering and panoscopic approach in p-type $ZrCoSb$ -based half-Heusler thermoelectric materials for achieving high ZT, *J. Mater. Chem. C* 4 (2016) 5766–5778.
- [31] N.S. Chauhan, S. Bathula, A. Vishwakarma, R. Bhardwaj, K.K. Johari, B. Gahtori, A. Dhar, Enhanced thermoelectric performance in p-type $ZrCoSb$ based half-Heusler alloys employing nanostructuring and compositional modulation, *J. Materiomics* 5 (1) (2019) 94–102.
- [32] H. Zhu, R. He, J. Mao, Q. Zhu, C. Li, J. Sun, W. Ren, Y. Wang, Z. Liu, Z. Tang, A. Sotnikov, Z. Wang, D. Broido, D.J. Singh, G. Chen, K. Nielsch, Z. Ren, Discovery of $ZrCoBi$ based half Heuslers with high thermoelectric conversion efficiency, *Nat. Commun.* 9 (2018) 2497.
- [33] P. Blaha, K. Schwarz, G.K.H. Madsen, D. Kvasnicka, and J. Luitz, WIEN2k: an Augmented Plane Wave Plus Local Orbitals Program for Calculating Crystal Properties. ISBN 39501031-1-2.
- [34] P. Blaha, K. Schwarz, P. Sorantin, S.B. Trickey, Full-potential, linearized augmented plane wave programs for crystalline systems, *Comput. Phys. Commun.* 59 (1990) 399–415.
- [35] J.P. Perdew, J.A. Chevary, S.H. Vosko, K.A. Jackson, M.R. Pederson, D.J. Singh, C. Fiolhais, Atoms, molecules, solids, and surfaces: applications of the generalized gradient approximation for exchange and correlation, *Phys. Rev. B* 46 (1992) 6671.
- [36] J.P. Perdew, K. Burke, M. Ernzerhof, Generalized gradient approximation made simple, *Phys. Rev. Lett.* 77 (1996) 3865.
- [37] U. von Barth, L. Hedin, A local exchange-correlation potential for the spin polarized case I, *J. Phys. C Solid State Phys.* 5 (13) (1972) 1629–1642.
- [38] M. Jamal, Cubic-elastic. http://www.WIEN2k.at/reg_user/unsupported/cub_ic-elast/, 2012.
- [39] G.K.H. Madsen, D.J. Singh, Boltztrap. A code for calculating band structure dependent quantities, *Comput. Phys. Commun.* 175 (2006) 67–71.
- [40] F.D. Murnaghan, The compressibility of media under extreme pressures, *Proc. Natl. Acad. Sci. U.S.A.* 30 (1944) 244–247.
- [41] M. El Amine Monir, H. Baltach, A. Abdiche, Y. Al-Douri, R. Khenata, S.B. Omran, X. Wang, D.P. Rai, A. Bouhemadou, W.K. Ahmed, C.H. Voon, Doping-induced half-metallic ferromagnetism in vanadium and chromium-doped alkali oxides K_2O and Rb_2O : ab initio method, *J. Supercond. Nov. Magnetism* 30 (2017) 2197–2210.
- [42] A. Togo, L. Chaput, I. Tanaka, Distributions of phonon lifetimes in Brillouin zones, *Phys. Rev. B* 91 (2015) 094306.
- [43] M. Born, K. Huang, *Dynamical Theory and Experiment*, I, Springer Verlag, Berlin, 1982.
- [44] F. Litimein, R. Khenata, A. Bouhemadou, Y. Al-Douri, S.B. Omran, First-principle calculations to investigate the elastic and thermodynamic properties of $RBRh_3$ (R = Sc, Y and La) perovskite compounds, *Mol. Phys.* 110 (2) (2011) 121–128.
- [45] I.R. Shein, A.L. Ivanovskii, Elastic properties of mono- and polycrystalline hexagonal AlB_2 -like diborides of s, p and d metals from first-principles calculations, *J. Phys. Condens. Matter* 20 (1) (2008) 415218, 415218(9).
- [46] S. Ghemid, S. Oundadji, H. Meradji, S. Drablia, S. Labidi, (FP-LPAW) Investigation of ternary alloys: $CdS_{1-x}Te_x$, *Phys. Procedia* 2 (2009) 881–887.
- [47] F. Zerarga, D. Allali, A. Bouhemadou, R. Khenata, B. Deghfel, S.S. Essaoud, R. Ahmed, Y. Al-Douri, S.S. Safaa, S.B. Omran, S.H. Naqib, Ab initio study of the pressure dependence of mechanical and thermodynamic properties of $GeB2O4$ (B = Mg, Zn and Cd) spinel crystals, *Comput. Condens. Matter*. 32 (2022) e00705.
- [48] S.F. Pugh, Relations between the elastic moduli and the plastic properties of Polycrystalline pure metals, *Philos. Mag. A* 45 (1954) 823–843.
- [49] I. Frantsevich, F. Voronov, S. Bokuta, *Elastic Constants and Elastic Moduli of Metals and Insulators Handbook*, Naukova Dumka, Kiev, 1983, pp. 60–180.
- [50] N. Guechi, A. Bouhemadou, R. Khenata, S.B. Omran, M. Chegaar, Y. Al-Douri, A. Bourzami, Structural, elastic, electronic and optical properties of the newly synthesized monoclinic Zintl phase $BaIn_2P_2$, *Solid State Sci.* 29 (2014) 12–23.
- [51] A. Bouhemadou, R. Khenata, F. Zerarga, Prediction study of structural and elastic properties under pressure effect of CdX_2O_4 (X = Al, Ga, In) spinel oxides, *Comput. Mater. Sci.* 39 (3) (2007) 709–712.
- [52] F. Belkharroubi, A. Mohammed, D. Bensaid, M. Noureddine, I. Ameri, S. Mesbah, Y. Al-Douri, Structural, magnetic, electronic and mechanical properties of full-Heusler alloys Co_2YAl (Y = Fe, Ti): first principles calculations with different exchange-correlation potentials, *J. Magn. Magn. Mater.* 448 (2018) 208–220.
- [53] R.J. Soulen Jr., J.M. Byers, M.S. Osofsky, B. Nadgorny, T. Ambrose, S.F. Cheng, P. R. Broussard, C.T. Tanaka, J. Nowak, J.S. Moodera, Measuring the spin polarization of a metal with a superconducting point contact, *Science* 282 (1998) 85–88.
- [54] G.D. Liu, X.F. Dai, H.Y. Liu, J.L. Chen, Y.X. Li, Gang Xiao, G.H. Wu, Mn_2Co_2Z (Z = Al, Ga, In, Si, Ge, Sn, Sb) compounds: structural, electronic, and magnetic properties, *Phys. Rev. B* 77 (2008) 014424.
- [55] C. Wood, Materials for thermoelectric energy conversion, *Rep. Prog. Phys.* 51 (4) (1988) 459.